Systematic calculations of plasma transport coefficients for the Periodic Table

George A. Rinker
Theoretical Division, Los Alamos National Laboratory, Los Alamos, New Mexico 87545
(Received 28 July 1987)

Theoretical results are given for the ionization state, electrical conductivity, thermal conductivity, and thermoelectric coefficient for the entire Periodic Table over extreme ranges of temperature and density. A spherical average ion embedded in a uniform plasma background is used as a model to evaluate the electron densities of states, elastic scattering cross sections, and ionization states. These are then combined with one-component plasma structure factors to compute mean relaxation times and electrical resistivities according to an extended Ziman formula. The method of Lampe is used to compute thermal conductivities and thermoelectric coefficients from these values. Some experimental comparisons are made. The transport coefficients appear to be accurate for weakly and moderately correlated plasmas, but not for strongly correlated liquids or crystalline materials. The coefficients are tabulated as numerical functions of temperature and density. The tables extend in temperature from 10^{-2} to 10^{4} eV. Density ranges depend upon atomic mass; lower limits range from 10^{-4} to 10^{-2} g/cm^3, and upper limits range from 10^{5} to 10^{7} g/cm^3. Indications are given of the regions of validity of the results.

I. INTRODUCTION

The extended Ziman formula for mean relaxation time or electrical resistivity may be derived from several different points of view. It is perhaps most simply shown to be valid in the weak scattering limit as a diffractive correction to the classical kinetic formula[1] or to the elementary solution of the Boltzmann equation.[2] The resistivity formula may be shown to be an upper bound derived from a variational solution of the Boltzmann equation.[2] Other direct approaches allow for strong scattering but require an interstitial region of free-electron propagation,[3] or show numerical equivalence to corresponding solutions of the Lenard-Balescu equation.[4] These analyses indicate that the extended formula is valid in general in the low-density limit for scattering of any strength, but quantitative bounds on its validity have not been established.

The purpose of the present work is to describe systematic results of a consistent theoretical application of the Ziman formula over the Periodic Table. We have no adjustable parameters in the calculation of relaxation time, although there is some latitude in the initial choice of potential for each element. The resistivity contains additional physical assumptions about the density of charge carriers. We have adopted the Boltzmann expression for this density by factoring the variational resistivity formula. However, the general accuracy of this expression is not clear, and some alternatives are discussed. Our principal intent in separating the discussion of mean relaxation time from resistivity and charge carrier density is to aid in physical interpretation and in some manipulations of the results. We are interested in extreme ranges of temperature and density, as shown schematically in Fig. 1, and a wide variety of elements and mixtures. Earlier forms of this model have been explored previously[5,6] A plane-wave approximation to it has been applied systematically over the entire Periodic Table.[7] The new aspects of the present work are some improvements in the physical model, the extensive results, and new comparisons with dense plasma experiments.

Besides use of the Ziman formula itself, our principal approximation arises from the assumed geometry. Spherical, average ionic potentials, which in some sense represent "typical" ions in the material, are used to generate the electron-ion cross sections and densities of states. This approximation is difficult to justify whenever there exists long-range ionic order, such as for crystals or strongly correlated liquids. For crystals, the appropriate basis states are periodic Bloch states rather than spherical-wave scattering states. For strongly correlated liquids, more success is obtained with cluster methods, which allow an electron to interact with more

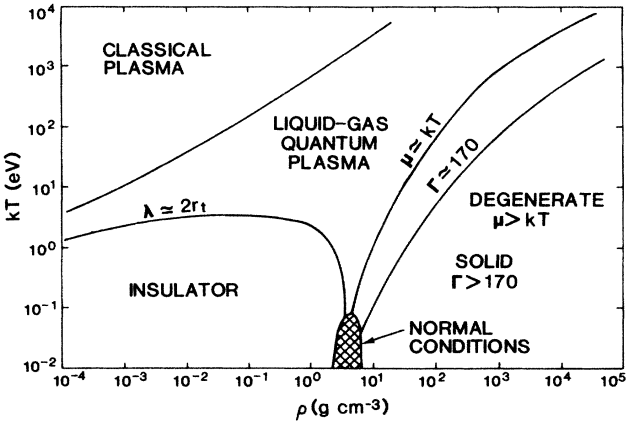

FIG. 1. Physical regions for iron in the temperature-density plane.

than one ion at a time.[8] Various adjustments[5] to the present approach have been explored (see Sec. III D) in attempts to correct for these shortcomings, but systematic success has been limited to moderately or weakly correlated systems.

The temperature-density space displayed in Fig. 1 may be divided into several distinct physical regions. At high temperature and low density, kinetic energies and ionic spacings are large, and we expect classical approximations to be valid. Quantum-mechanical effects become important at lower temperature and higher density, where the average ionic spacing is no longer large compared with electron wavelengths. At still lower temperatures, the electron mean free path becomes comparable with ionic spacing, ionization vanishes, and the material becomes insulating. As the density is increased, pressure ionization eventually dominates any thermal ionization, and the electrons become degenerate. Crystallization occurs; one-component-plasma simulations indicate that lattices are formed in general when the ion-ion coupling constant Γ reaches $\simeq 170$.

The small region marked "normal conditions" poses particularly delicate calculational problems. The liquid-solid and metal-insulator phase transitions converge here. The free energy reaches a global minimum, indicating a balance among internal atomic forces within the material and zero pressure at finite density. This balance among competing effects means that any calculated physical parameters are sensitive to the precise electronic wave functions, requiring detailed representation of the conduction bands. For some special cases, errors in the present model are not important and reasonable results are obtained, but for normal conditions this is the exception rather than the rule.

II. MODEL DETAILS

The electron states are found by solving the Dirac equation numerically in a local, continuous, spherical electron-ion potential $V(r)$, with exterior boundary condition $V(r)=V(r_t)$ for $r \geq r_t$. The Wigner-Seitz radius r_t is defined in terms of the atomic volume $\Omega=4\pi r_t^3/3$. The chemical potential μ is determined by charge neutrality:

$$Z=\int_{-m}^{\infty} d\varepsilon f_{\beta\mu}(\varepsilon)\frac{dN(\varepsilon)}{d\varepsilon} , \tag{1}$$

where $p^2+m^2=(\varepsilon+m)^2$ defines the exterior momentum p (wave number) and kinetic energy ε, $f_{\beta\mu}(\varepsilon)$ is the Fermi-Dirac distribution function for inverse temperature $\beta=1/kT$, and we use natural units $\hbar=c=1$. We have chosen the zero of energy ε at the external potential value $V(r_t)$, so that setting the lower limit of the integral to $-m$ includes the bound-electron states. We use the Dirac equation only to obtain accurate radial wave functions; subtleties due to relativistic exchange and vacuum polarization are ignored. The density of electron states $dN(\varepsilon)/d\varepsilon$ is computed by partial-wave analysis of the explicit solutions of the Dirac equation for angular momenta $|\kappa| \leq \kappa_{\max}(\varepsilon) \leq 96$, where $\kappa_{\max}(\varepsilon)$ depends upon internal convergence parameters. The remainder of the series is summed in the Fermi gas approximation for each energy.

The extended Ziman formula for the mean relaxation time τ is[1-3]

$$\frac{1}{\tau}=\frac{1}{3\pi m Z_0}\int_0^{\infty} d(\beta\varepsilon) f_{\beta\mu}(\varepsilon)[1-f_{\beta\mu}(\varepsilon)]\Sigma(\varepsilon) , \tag{2}$$

where

$$\begin{aligned} Z_0&=\frac{\Omega}{3\pi^2}\int_0^{\infty} d(\beta\varepsilon) f_{\beta\mu}(\varepsilon)[1-f_{\beta\mu}(\varepsilon)]p^3 \\ &=\frac{\Omega}{\pi^2}\int_0^{\infty} d\varepsilon f_{\beta\mu}(\varepsilon)(\varepsilon+m)p \end{aligned} \tag{3}$$

may be interpreted as the number of free electrons per atom (ionization state), and

$$\Sigma(\varepsilon)=\int_0^{2p} dq\, q^3 S(q)\sigma_{\varepsilon}(q) . \tag{4}$$

The relaxation time is often discussed in terms of the mobility $e\tau/m$. The principal difference between these equations and the original Ziman formulation lies in the partial-wave analysis and the extension to finite temperature. Equation (3) is a finite-temperature generalization of a factor (Fermi-surface radius)$\times$(Fermi-surface area). It reduces in the degenerate limit to the usual result $Z_0/\Omega=p_F^3/3\pi^2$ and is required to have this form by the variational derivation of the Ziman formula.[2] The electron-ion elastic scattering cross section $\sigma_{\varepsilon}(q)$ for momentum transfer $\mathbf{q}$ and incident energy ε is determined along with the density of states by partial-wave analysis in $V(r)$, with Born approximation used to sum the series beyond the angular momentum cutoff. The ionic structure factor $S(q)$ is interpolated from the tabulated values of Rogers *et al.*[9] for the one-component plasma. For values of Γ or q outside the published table, the appropriate table boundary values are used. This structure factor approaches the Debye-Hückel limit in the classical regime and the Percus-Yevick limit at melting point for liquid metals.

It is not difficult to show in both the degenerate and nondegenerate limits that the mean relaxation time Eq. (2) remains finite as $Z_0 \to 0$ at finite density. This occurs because the integrals in Eqs. (2) and (3) cancel each other as $Z_0 \to 0 (\beta\mu \to -\infty)$ apart from relatively slowly varying functions of ρ and T. This dependence is consistent with the classical kinetic formula. It is an important physical constraint required for consistency in the related transport coefficients.[5,10]

The electrical resistivity η is given in terms of the mean relaxation time as

$$\eta=\frac{1}{\sigma}=\frac{1}{\tau}\frac{m}{\alpha}\frac{\Omega}{Z_i} , \tag{5}$$

where σ is the electrical conductivity, $\alpha=1/137.03604$ is the fine-structure constant, and Z_i/Ω is the density of charge carriers. It may be argued on variational grounds[2] that if the identification $Z_i=Z_0$ is made, then Eq. (5) gives an upper bound for the resistivity when the Boltzmann equation is valid. In the classical kinetic picture,[1] however, these two factors have separate physical

origins. Z_0 arises from generalization of a factor p^3 and is required to have the form Eq. (3) (or its nonrelativistic version) if a meaningful relaxation time is to be defined. The factor Z_i/Ω arises from the relation between relaxation time and resistivity. Its value is not specified by kinetic theory. We find that in some regions of temperature-density space, our calculated relaxation times are more reasonable than the ionization states $Z_i=Z_0$. For this reason, we consider Z_i to be a physical parameter which is sometimes better obtained through other means. In order to maintain this distinction, we use the symbol Z_0 to represent the solution of Eq. (3), and Z_i to represent the factor in Eq. (5) even when it is set equal to Z_0.

Although the interior potential $V(r)$ for $r \leq r_t$ may be obtained from any source, we specialize in the present work to particular Dirac-Fock-Slater (DFS) and Thomas-Fermi-Dirac (TFD) models.[5] At low density and temperature, we use a self-consistent DFS potential $V_{\rm DFS}(r)$ for the isolated ion with the local Kohn-Sham exchange interaction. Except for the fact that exchange is treated approximately, this is correct in the zero-temperature, zero-density limit. At high temperature and density, the potential is a self-consistent TFD potential $V_{TFD}(r)$ with finite-density boundary conditions and elevated-temperature phase-space populations. This is correct in high-temperature, high-density limit. The same Kohn-Sham exchange interaction is used, but here it is added after self-consistency is reached in order to avoid some of the peculiarities of the isolated TFD ion. This makes no quantitative difference in the present work where the TFD model is justified.

In previous work, these potentials were calculated for neutral atoms, modified with the Latter approximation to have $-r^{-1}$ exterior boundary conditions, and cut off at r_t. This procedure is somewhat ambiguous, and it is not clear physically what such a potential represents. However, the $-r^{-1}$ behavior is quantitatively important. At low density it corresponds to the Hartree-Fock exterior boundary condition for the isolated atom. At high density we lack a physical interpretation but find that reasonable conduction bands are not obtained otherwise. In the present work, we achieve a similar result while avoiding the particular ambiguities of the Latter approximation by calculating self-consistent potentials for positive ions of charge $+1$. Electronic configurations are usually chosen in normal order, but these may be altered if necessary to provide more realistic densities of states near normal conditions.

In intermediate regions of temperature and density, the two potential models are superimposed according to an *ad hoc* algorithm

$$V(r)=a\,[V_{\rm DFS}(r)-V_{\rm DFS}(r_t)] + (1-a)[V_{\rm TFD}(r)-V_{\rm TFD}(r_t)]\ , \tag{6}$$

where

$$a=(1+T/T_0)^{-1}(1+\rho/\rho_0)^{-1}\ , \tag{7}$$

with $T_0=100$ eV and $\rho_0=100$ g/cm^3. The density ρ_0 corresponds to a total electron density of approximately 3×10^{25} cm^{-3} for any material. Because the DFS and TFD calculations are carried out for the same ionization state, the external boundary conditions are compatible, and the superposition passes smoothly from one limit to the other.

It is possible to make a conceptual improvement by using fully self-consistent potentials based upon solutions of the Dirac equation at each finite temperature and density. This level of self-consistency is feasible and has been applied successfully in other contexts in the past.[11] We have made extensive comparisons with such potentials and find noticeable differences in the transport coefficients only in the conductor-insulator transition regions. These differences do not represent systematic improvement in comparisons with experimental data, however. Evidently, the other defects in the present approach are more important. Use of these potentials introduces an additional dimension of complexity which makes it awkward to carry out calculations of the present scope. They are thus not used here except in isolated cases where fitting to individual elements is involved.

The partial-wave expansion converges too slowly to be useful in the classical region of high temperature and low density. Where internal numerical checks indicate nonconvergence, a modified plane-wave version[7] of the Ziman theory is substituted. These more approximate calculations are corrected and joined smoothly to the partial-wave results in the following way. Define the variables $x=Z_i/(Z-Z_i)$, $y=\eta Z_i/\Omega=m/\alpha\tau$. This transforms the ionization state into the variable range $0\leq x\leq\infty$ and removes the leading Z_i dependence from the resistivity. Multiplicative correction factors $C_{jk}=x(\rho,T)/x_a(\rho,T)$ or $y(\rho,T)/y_a(\rho,T)$ are then calculated wherever converged results are available, where j and k are grid indices in the (ρ,T) plane, x and y are the partial-wave results, and x_a and y_a are the approximate plane-wave values. The correction factors are extrapolated into the unknown density-temperature region with the algorithm

$$C_{jk}=\tfrac{1}{2}(C_{j+1,k}+C_{j,k-1})\ . \tag{8}$$

The grid is covered sequentially for decreasing ρ and increasing T, which ensures that the factors on the right side of Eq. (8) are available when needed. The correction factors are then used to construct new values of Z_i, τ, and η, which may be considered equivalently either as extrapolated partial-wave values, or as renormalized plane-wave values.

III. SELECTED RESULTS

A. Relaxation time and ion coupling

Figures 2 and 3 show the relaxation time τ and ion-ion coupling constant $\Gamma=Z_i^2\alpha\beta/r_i$ over the full temperature and density range for $_{50}$Sn. The rich structure in the relaxation time surface for small ρ and T reflects the electron behavior at threshold, as bound states pass to and from the continuum. This structure is interesting but

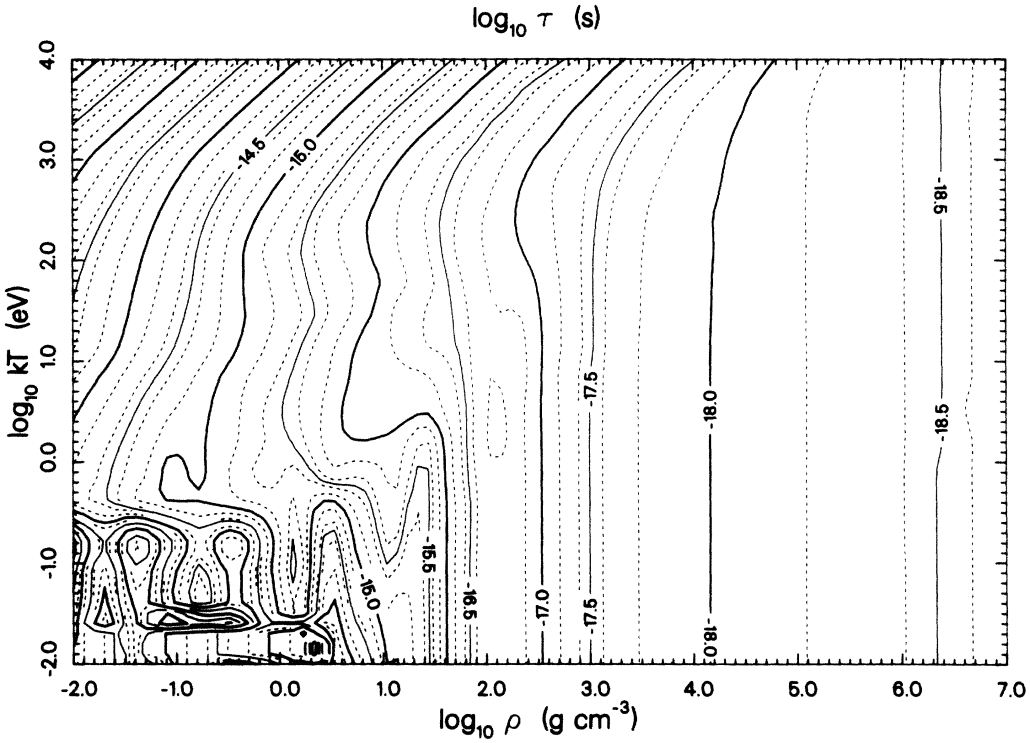

FIG. 2. Calculated mean relaxation time τ for $_{50}$Sn as a function of temperature and density.

not important except near the metal-insulator transition at $\rho \simeq 10$ g/cm^3, as the ionization states are so small that the material is generally insulating. At high temperature and low density, the expected logarithmic dependence upon T is observed.

The plot of Γ in Fig. 3 indicates regions of validity of the present results. The area between $\Gamma \simeq 1$ and $\Gamma \simeq 10^2$ is of primary interest, as here the plasma is moderately coupled, so that classical approximations are inadequate and the present results should represent substantial im-

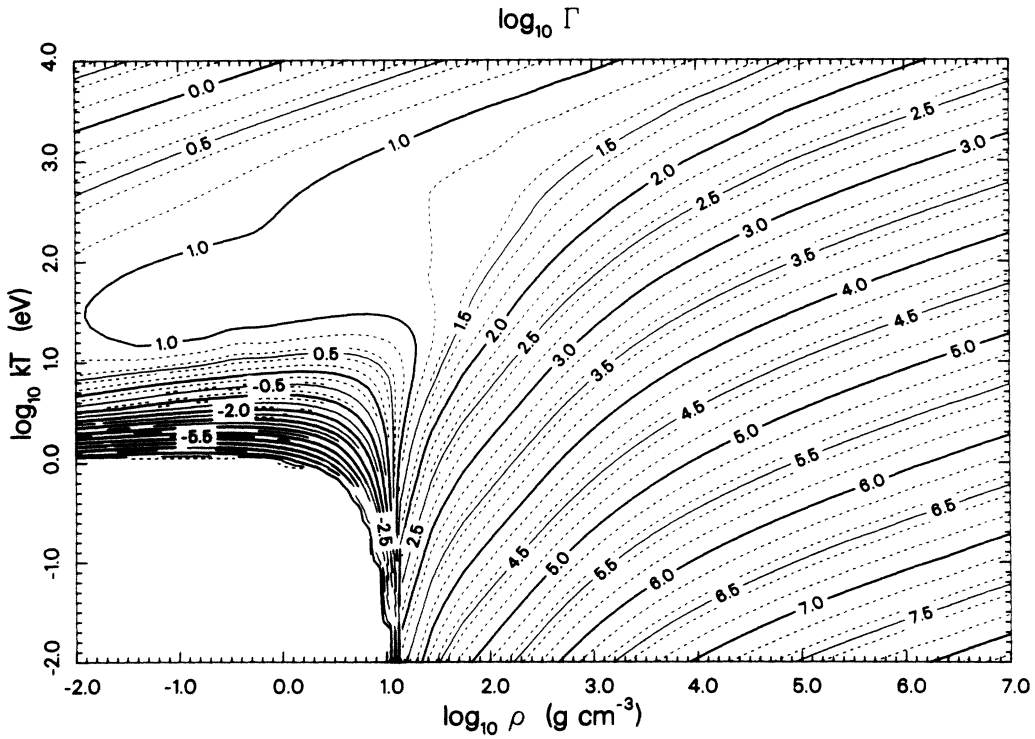

FIG. 3. Calculated ion-ion coupling constant Γ for $_{50}$Sn as a function of temperature and density.

provement. For values of Γ above $\simeq 10^2$ on the right side of the figure, the approximations used here are invalid and the results have only qualitative interest. Very small values of Γ delineate the insulating region.

B. Density of states

A possible point of contact and comparison is the electron density of states near normal conditions. Although we do not expect quantitative results, it is nevertheless interesting to see what qualitative features are reproduced. Figures 4–9 show some densities of states $dN(\varepsilon)/d\varepsilon$ and integrated densities of states $N(\varepsilon)$ for atomic numbers $Z=25$–30, at solid density and $kT=2.5\times10^{-2}$ eV (solid line), and liquid density at melting point (dashed line). The chemical potential μ for each case is indicated by an inverted triangle on the abscissa. Configurations used for calculating the DFS potentials are $3d^6$, $3d^7$, $3d^8$, $3d^9$, $3d^{10}$, and $4s^1$ for $Z=25$–30. These plots may be compared with band-structure calculations, such as in Ref. 12 for solid densities.

The prominent resonance in each case is due to the $3d$ electrons. In manganese, the chemical potential falls on the upper slope of the resonance, corresponding to a partially filled shell. This is qualitatively similar to the band-structure result, except in that case, the d states are split into three overlapping peaks of total width approximately 4 eV. Our results can be improved somewhat by broadening the resonance by this amount (see Sec. III D). However, the structure cannot be reproduced.

A small asymmetry is visible in the peak of our density of states for liquid iron, but again, this compares only crudely with the band structure result. The chemical potential is closer to threshold, resulting in a smaller free ionization state with $Z_i=Z_0$, but it is higher relative to the resonance centre. More structure is evident in cobalt, where the chemical potential has moved almost out of the resonance. The chemical potential is in the free-electron region above the resonances at both densities for nickel, where the fine structure is cleanly separated. This is to be contrasted to the solid density band-structure result, where the chemical potential remains at the upper edge of the resonance region. For copper, we find the d resonances to be truly bound at liquid density

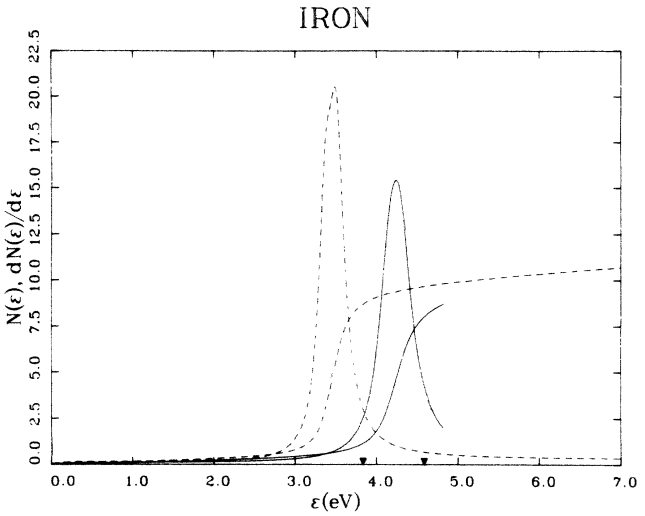

FIG. 5. Integrated density of states $N(\varepsilon)$ and density of states $dN(\varepsilon)/d\varepsilon$ for $_{26}$Fe at normal solid density 7.86 g/cm^3 and $kT=2.5\times10^{-2}$ eV (solid lines), and melting-point liquid density 7.05 g/cm^3 and temperature 0.156 eV (dashed lines). Inverted triangles on the abscissa indicate the chemical potential μ for each case.

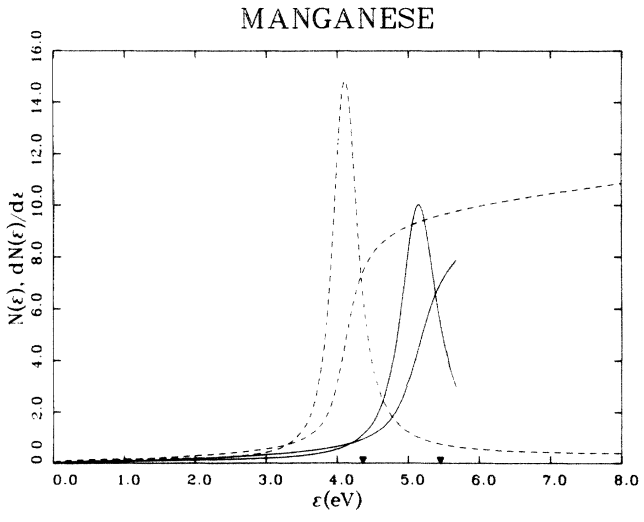

FIG. 4. Integrated density of states $N(\varepsilon)$ and density of states $dN(\varepsilon)/d\varepsilon$ for $_{25}$Mn at normal solid density 7.43 g/cm^3 and $kT=2.5\times10^{-2}$ eV (solid lines), and melting-point liquid density 6.43 g/cm^3 and temperature 0.131 eV (dashed lines). Inverted triangles on the abscissa indicate the chemical potential μ for each case.

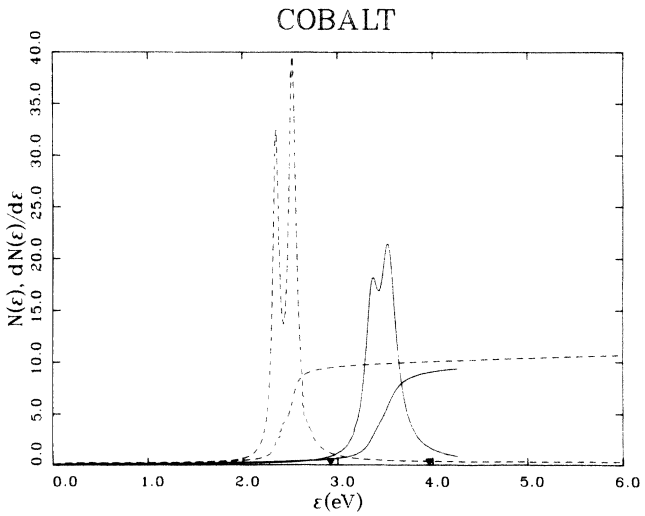

FIG. 6. Integrated density of states $N(\varepsilon)$ and density of states $dN(\varepsilon)/d\varepsilon$ for $_{27}$Co at normal solid density 8.90 g/cm^3 and $kT=2.5\times10^{-2}$ eV (solid lines), and melting-point liquid density 7.72 g/cm^3 and temperature 0.152 eV (dashed lines). Inverted triangles on the abscissa indicate the chemical potential μ for each case.

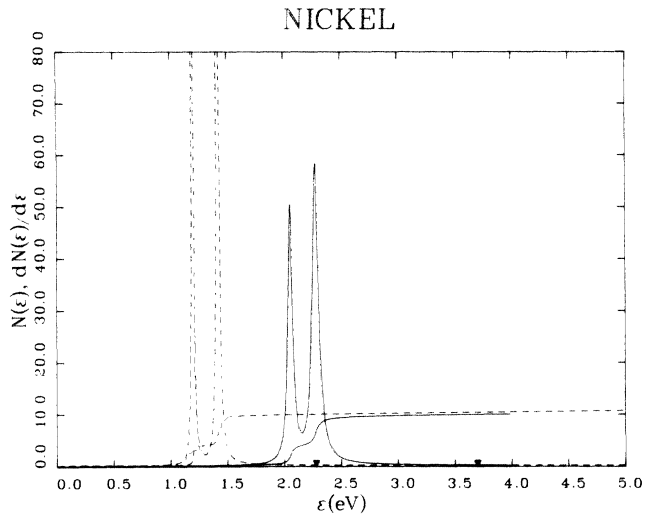

FIG. 7. Integrated density of states $N(\varepsilon)$ and density of states $dN(\varepsilon)/d\varepsilon$ for $_{28}$Ni at normal solid density 8.90 g/cm^3 and $kT=2.5\times10^{-2}$ eV (solid lines), and melting-point liquid density 7.85 g/cm^3 and temperature 0.149 eV (dashed lines). Inverted triangles on the abscissa indicate the chemical potential μ for each case.

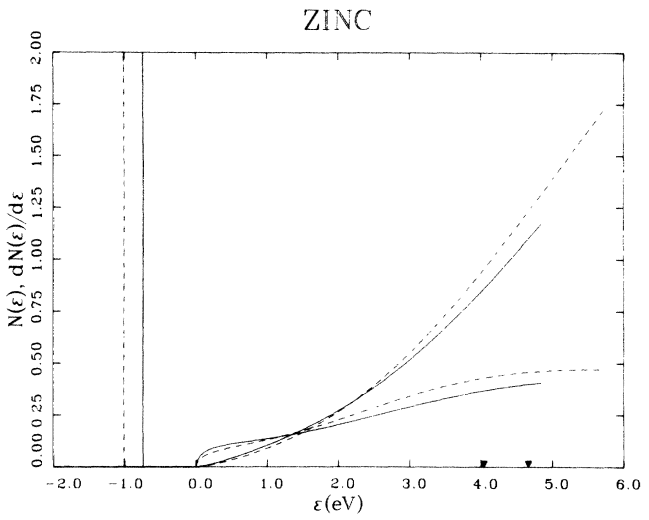

FIG. 9. Integrated density of states $N(\varepsilon)$ and density of states $dN(\varepsilon)/d\varepsilon$ for $_{30}$Zn at normal solid density 7.14 g/cm^3 and $kT=2.5\times10^{-2}$ eV (solid lines), and melting-point liquid density 6.61 g/cm^3 and temperature 0.060 eV (dashed lines). Inverted triangles on the abscissa indicate the chemical potential μ for each case.

and nearly bound at solid density, although the distinction is not important because the chemical potentials are high enough that the conduction electrons are nearly free at both densities. The resonances are bound at both densities for zinc, where the free-electron conduction behavior persists.

C. Ionization and resistivity

Table I shows calculated values of Z_0 and η for the same elements compared with available measurements.[13]

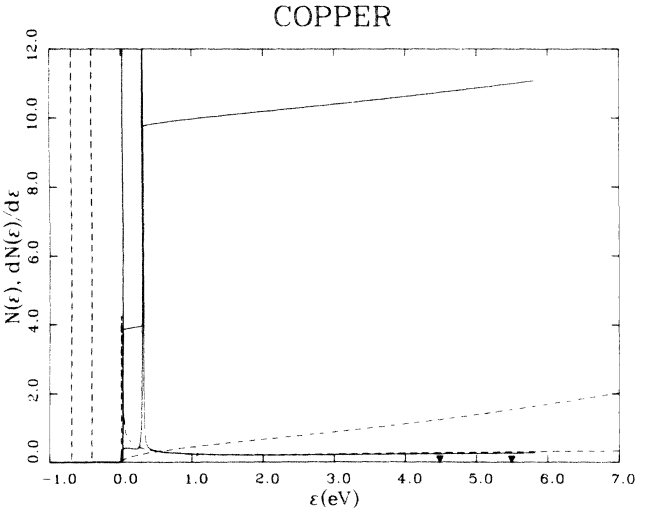

FIG. 8. Integrated density of states $N(\varepsilon)$ and density of states $dN(\varepsilon)/d\varepsilon$ for $_{29}$Cu at normal solid density 8.96 g/cm^3 and $kT=2.5\times10^{-2}$ eV (solid lines), and melting-point liquid density 7.96 g/cm^3 and temperature 0.117 eV (dashed lines). Inverted triangles on the abscissa indicate the chemical potential μ for each case.

Resistivities for two choices of Z_i are shown. The qualitative trends from strong scatterer to nearly free-electron metal are reproduced in the calculations with $Z_i=Z_0$ (column 5), but the calculated resistivities are generally too large by factors of 2–5 or more. There are a variety of possible reasons for this. One may be that the ionization states are too small. A uniform increase by a factor of 3 in Z_i would improve agreement considerably. The results are perhaps more consistent for the liquids, where the detailed geometrical effects of band structure are less important. The best resistivities are obtained for copper and zinc. Here in the conduction band the electron-ion interaction is weak, so that the multiple scattering effects neglected in the Ziman formula are less important.

In column 6 of Table I we consider an alternative definition $Z_i=Z_c$, where Z_c is the number of continuum electrons ($\varepsilon>0$), evaluated from Eq. (1) with the lower limit of the integral set to 0. This choice results in ionization states that are generally too large and resistivities that are too small. The physical reason for this is that states that are formally in the continuum may nevertheless behave more like bound states if they resonate strongly in the ionic potential. This binding effect is largest for the transition metals, where the errors are as large as for the choice $Z_i=Z_0$, but in the opposite direction. To some extent this phenomenon is incorporated in our calculation of relaxation time. However, our complete reliance upon scattering states is an approximation which makes the physical picture ambiguous. Evidently the best answer usually lies somewhere between the two extremes Z_0 and Z_c.

A better point of comparison may be made at higher temperature. One reason for this is that electron kinetic energies are larger compared with their interactions with the ions, so that the scattering is effectively weaker and

TABLE I. Ionization state Z_0 and resistivity η for two choices of Z_i for atomic numbers $Z=25-30$, at solid and liquid densities and temperatures. Experimental values are from Ref. 13.

			Solid (normal conditions[a])			
$_ZX$	ρ (g/cm^3)	kT (eV)	Z_0	$\eta(Z_i=Z_0)$ ($\mu\Omega$ cm)	$\eta(Z_i=Z_c)$ ($\mu\Omega$ cm)	η(expt) ($\mu\Omega$ cm)
$_{25}$Mn	7.43	0.025	0.71	240	24	185
$_{26}$Fe	7.86	0.025	0.53	81	8.2	9.7
$_{27}$Co	8.90	0.025	0.39	18	0.8	6.2
$_{28}$Ni	8.90	0.025	0.35	4.9	0.2	6.8
$_{29}$Cu	8.96	0.025	0.69	6.1	0.7	1.7
$_{30}$Zn	7.14	0.025	0.69	28	18	5.9
			Liquid (melting point)			
$_ZX$	ρ (g/cm^3)	kT (eV)	Z_0	$\eta(Z_i=Z_0)$ ($\mu\Omega$ cm)	$\eta(Z_i=Z_c)$ ($\mu\Omega$ cm)	η(expt) ($\mu\Omega$ cm)
$_{25}$Mn	6.43	0.131	0.59	640	54	174
$_{26}$Fe	7.05	0.156	0.45	423	24	139
$_{27}$Co	7.72	0.152	0.29	281	9.1	102
$_{28}$Ni	7.85	0.149	0.20	440	8.6	85
$_{29}$Cu	7.96	0.117	0.57	45	20	21
$_{30}$Zn	6.61	0.060	0.60	90	57	37

[a]Values of Z_0 and η are calculated for the solid at $kT=2.5\times10^{-2}$ eV. The experimental measurements are taken at various other temperatures. This distinction is unimportant because the theoretical results are nearly independent of temperature below melting point.

more elastic. Another is that fine structure in the electron states is less important because their populations are spread over more states. A third is that electron wavelengths are shorter, so that classical conditions are more closely approached, and a diffractive approximation may be more realistic. Finally, Z_0 approaches Z_c at high temperature, and the ambiguity with respect to ionization state becomes less important.

There are very few direct measurements outside of the purely classical regime at temperatures of order several eV or more. One recent measurement has been made by Shepherd[14] for a predominantly hydrocarbon plastic at approximately 10 eV and solid density (2.7 g/cm^3). This measurement is made by discharge of a 500 kA electrical current through a 20 μm hole in the solid. His resistivity measurements for this device as a function of time are shown in Fig. 10. Also shown are results of several calculations for the temperature and density maintained throughout most of the experiment. The dashed line was taken from a previous report[6] of the present methods applied to the mixture C_2H_3, using the earlier potential model described above. The other labeled curves are Shepherd's evaluations of the Spitzer model[15] and of the theory of Ichimaru *et al.*[16]

The discrepancy between experiment and the Spitzer model is interesting in that it illustrates the extent to which the classical approach is invalid at these conditions. The discrepancy with Ichimaru *et al.* is more subtle. In a series of papers, these authors have developed a comprehensive treatment based upon the two-component plasma. They derive an expression which reduces to the Ziman formula at $T=0$ but otherwise represents a different generalization to finite temperature than used here. They represent the electron-ion interaction in Born approximation, using a Coulomb potential $-Z_i\alpha/r$ with dielectric screening. They assume the value $Z_i=1$ rather than attempt to calculate it. Finally, they renormalize their calculated conductivity by a factor 1.97 in order to compensate for observed errors in the classical limit. The model simplifications may be the source of the discrepancy, particularly the assumption of the value $Z_i=1$, and secondarily, the questionable electron-ion interaction. In the present calculation, the average value of $Z_i=Z_0$ obtained from Eq. (3) is 0.28 per atom. Because the conductivity is approximately linear in Z_i, this smaller value makes a substantial difference. Altering the present calculation to correspond to $Z_i=1$ without changing the relaxation time yields a resistivity of 5.3×10^{-4} Ω cm, in closer agree-

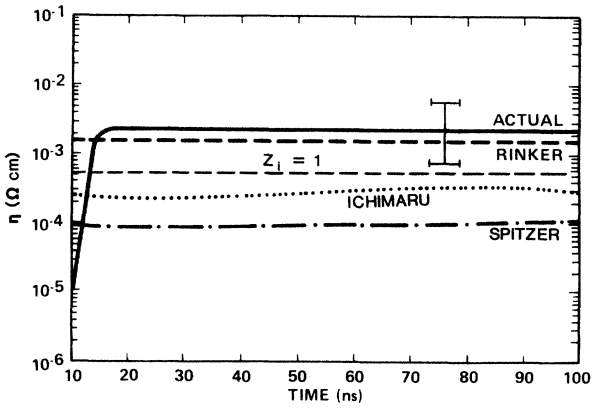

FIG. 10. Measured resistivity of plastic at $kT=10$ eV and $\rho=2.7$ g/cm^3, compared with various theoretical calculations for C_2H_3 at the same temperature and density.

ment with that of Ichimaru *et al.* but in worse agreement with experiment. It should be emphasized that the physical ionization state Z_i is difficult to calculate reliably under these conditions, which are near the conductor-insulator transitions. It is a rapidly varying function of temperature and density, and relatively small variations in the model can lead to larger changes in Z_i than in τ.

Further comparisons may be made with experiments at somewhat lower temperatures and densities.[17] In these experiments, an explosively driven shock wave propagates through an inert gas which is at an initial pressure of 0.25 to 30 bar. Apparently the only directly measured parameters are the shock velocity and electrical conductivity. The other parameters (ion density, electron density, temperature, and pressure) are inferred from the conservation equations and model ionization rates and equations of state.[18] These derived temperatures and densities (uniformly assuming $Z_i = 1$) and measured conductivities are listed for three gases in Table II. Also shown in the last column are the results of Ichimaru *et al.*, who show excellent agreement in all cases. The fifth column in Table II shows results of the present calculation under the same uniform assumption $Z_i = 1$. Agreement is also excellent for Ne and Ar but not for Xe. The reason for the latter discrepancy is not clear. The numbers are all too small by an approximate factor of 2, suggesting that the true ionization state is closer to 2 than 1. This makes physical sense because Xe has many more electrons than Ne and Ar, and the Xe experiments are carried out at higher temperatures and densities. Some caution should be applied, however, as different ionization states would alter the entire interpretation of the pressures, temperatures, and densities in the experiment. It is also not clear why the present calculations should agree with Ichimaru *et al.* for Ne and Ar but no Xe. It should be pointed out further that the ionization states $Z_i = Z_0$ calculated by the present method are evidently incorrect. They are much smaller, ranging from 0.01 to 0.2, and would lead to conductivities which are inconsistent with the measurements.

D. Semiempirical corrections

One of the most fundamental problems with the present approach is the inaccurate electron structure that can result from the average spherical ion approximation. In a real plasma, local temperature and density fluctuations and ion motion contribute to the broadening of continuum resonances and some bound states. Static geometrical effects in the solid or strongly correlated liquid alter their structure. This problem is not so acute at high temperature, where the electron populations are spread over many different states, nor at high density, where the states involved in transport are nearly free. At low temperature near the metal-insulator and liquid-solid phase transitions, however, the calculated density of states and cross section can be very unrealistic. This can lead to ionization states and resistivities which are in serious disagreement with experiment.

There appears to be no demonstrably correct method to remedy these deficiencies in general without resorting directly to calculations with ensembles of ions or periodic electron states. We have attempted simpler corrections in four different ways. The first and most straightforward is by adjusting the electron-ion potential. Within limits it is possible to locate the important electron states at approximately the correct energies by changing configurations in the DFS calculations. This procedure is useful where the band structure is already known, but it creates significant and unpredictable effects elsewhere, and it does not address the problem of resonance broadening and fragmenting.

The second uses the physically motivated convolution procedure described previously.[5] This consists of the replacement

TABLE II. Experimental and theoretical values for electrical conductivities of inert gases at elevated temperature. Measurements are from Ref. 17; densities, temperatures, and conductivities are interpreted and calculated assuming average ionization state $Z_i = 1$.

Gas	ρ (mg/cm^3)	kT (eV)	σ(expt) (Ω^{-1} cm^{-1})	σ(calc) (Ω^{-1} cm^{-1})	σ^a (Ref. 16) (Ω^{-1} cm^{-1})
$_{10}$Ne	0.37	1.71	130	150	148
	0.64	1.69	165	168	160
$_{18}$Ar	1.9	1.91	190	192	200
	3.7	1.75	155	204	203
	5.4	1.66	170	209	209
	9.3	1.64	255	246	234
	11	1.53	245	241	232
$_{54}$Xe	55	2.59	450	223	442
	130	2.37	680	241	506
	170	2.33	740	262	546
	310	2.25	690	368	657
	350	2.16	780	371	660
	440	2.12	1040	481	728
	440	1.96	930	476	694

[a]Includes a normalization factor 1.97 to guarantee convergence to the classical limit.

$$g(p) \rightarrow \int_{-\infty}^{\infty} dp' g(p') h_\gamma(p'-p) , \quad (9)$$

where $g(p)$ is proportional to either of the functions $dN(\varepsilon)/d\varepsilon$ or $\Sigma(\varepsilon)$, and $h_\gamma(q)$ is a convolution function of characteristic width γ. It is not important whether the above integral is carried out in energy space or in momentum space. So long as γ is small and the function $h_\gamma(q)$ falls off rapidly enough, there is no quantitative difference. A more significant question concerns the choice of functions $g(p)$. In principle, one may extract leading powers of p (or ε) and reinsert them after convolution. This determines the threshold behavior of the resulting functions, and can yield densities of states that are constant or diverge at threshold.

Dimensional arguments suggest that the convolution width γ in momentum space should be of order r_t^{-1}. A better argument notes that between scatterings, an electron is localized to within $\sim\lambda$ (the mean free path), so that its momentum is uncertain by $\gamma \sim \lambda^{-1}$. Other qualitative arguments may be made, but it must be emphasized that this is an empirical procedure with limited predictive power. For example, it is straightforward to distribute the resonance strength in Figs. 4–9 by any desired amount, but the result is always a smooth peak instead of the fragmented band-structure result.

It should be noted that the Lorentzian functions used in some previous calculations are inappropriate for most choices of $g(p)$ because their long-range tails render the integrals Eq. (9) divergent. In current work, we choose an exponential form in momentum

$$h_\gamma(q) = \frac{\ln 2}{\gamma} e^{-|p'-p| 2\ln 2/\gamma} , \quad (10)$$

where γ is the full width at half maximum.

A third approach is a simplified approximation to the above, in which the convolution Eq. (9) is not carried out explicitly but the temperature is modified to represent the broadening.[5] This is computationally more efficient, but it offers less control of the model and can lead to further unphysical results. For these reasons, this approach has been abandoned in current work.

A fourth approach involves the direct calculation of some effects of density and temperature fluctuations. The probability W of a fluctuation in a small domain is given by[19]

$$\ln(W/K) \simeq -\Delta G/T , \quad (11)$$

where K is a normalization constant and

$$\Delta G = \Delta E - T\,\Delta S + P\,\Delta V - \mu\,\Delta N \quad (12)$$

is the associated change in Gibbs free energy. Calculation of this probability is complicated by the fact that at equilibrium, the free energy is stationary in the thermodynamic variables, so that the terms linear in the deviations must cancel. In order to insure this cancellation, we use a simple analytic model of an electron-ion ideal gas of $N = Z_i + 1$ particles per atom. The probability is then

$$\ln(W/K) \simeq -\frac{3N}{4}\left[\frac{\Delta T}{T}\right]^2 - \frac{N}{2}\left[\frac{\Delta V}{V} - \frac{\Delta N}{N}\right]^2 . \quad (13)$$

We view the material as a mixture of ions of varying temperature, size, and number of particles. Each ion has associated with it the values of Z_i and τ calculated with our homogeneous model. The calculated functions are integrated with the probability function W over the region surrounding the temperature and density of interest. The ionization state is averaged linearly,

$$\langle Z_i(\rho_0, T_0)\rangle = \int d\rho \int dT\, W(\Delta\rho, \Delta T) Z_i(\rho, T) . \quad (14)$$

The relaxation time is averaged inversely[2],

$$\langle \tau^{-1}(\rho_0, T_0)\rangle = \int d\rho \int dT\, W(\Delta\rho, \Delta T) \tau^{-1}(\rho, T) . \quad (15)$$

Averaging the resistivity linearly or inversely corresponds to the ions acting as conductors in series or parallel, respectively. Neither picture is actually appropriate because the directionality of any current flow introduces a detailed dependence upon the internal geometry of the material (violation of Mattheissen's rule). More complicated methods for combining mixtures have been studied by Landauer.[20] We have adopted the above procedure because we believe that it is more important to maintain the relaxation time and leading dependence $\sigma = \eta^{-1} \propto Z_i$.

Figures 11–16 show some sample comparisons of these modifications at intermediate temperatures. Figures 11 and 12 show the ionization state $Z_i = Z_0$ and mean relaxation time τ calculated for carbon over a restricted range of temperature and density, in the regions of the thermal and pressure conductor-insulator transitions. The DFS configuration is $1s^2 3d^3$, chosen[6] to produce appropriate band gaps at diamond and graphite densities. Figures 13 and 14 display results of the same calculation carried out using the DFS configuration $1s^2 2s^2 2p^1$. There is little difference in Z_i over most of the region where it is not small. The principal effect is in moving the conductor-insulator transitions to temperatures and densities that are lower by approximate factors of 2. Fractional changes at this boundary and in the insulating region are large because the absolute values of the functions are small. There is some change in the structure of the relaxation time surface, principally in the region of small Z_i.

The same calculation with convolution of the functions $dN(\varepsilon)/d\varepsilon$ and $\Sigma(\varepsilon)$ using the width $\gamma^{-1} = 4r_t$ in momentum space produces no noticeable change in this region of temperature and density. Except for a depression of approximately 20% around $\rho = 4$ g/cm^3 and $kT = 4$ eV, the calculation agree to within a few percent or less.

Figures 15 and 16 show effects of fluctuations. There is again little change in Z_i except near the conductor-insulator transitions, which are moved to lower temperature and densities. The structure of the relaxation time surface is smoothed considerably with no major changes in absolute magnitude.

Table III compares the last two modifications with the

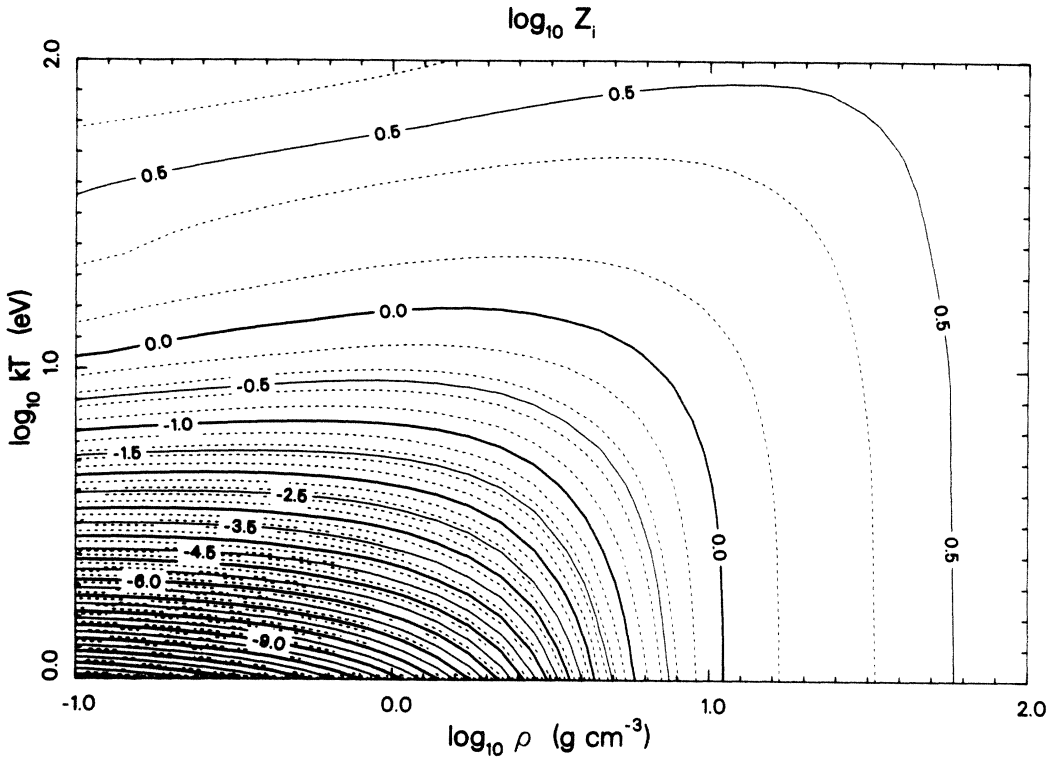

FIG. 11. Ionization state Z_i of carbon near the conductor-insulator transitions, calculated with DFS potential configuration $1s^2 3d^3$.

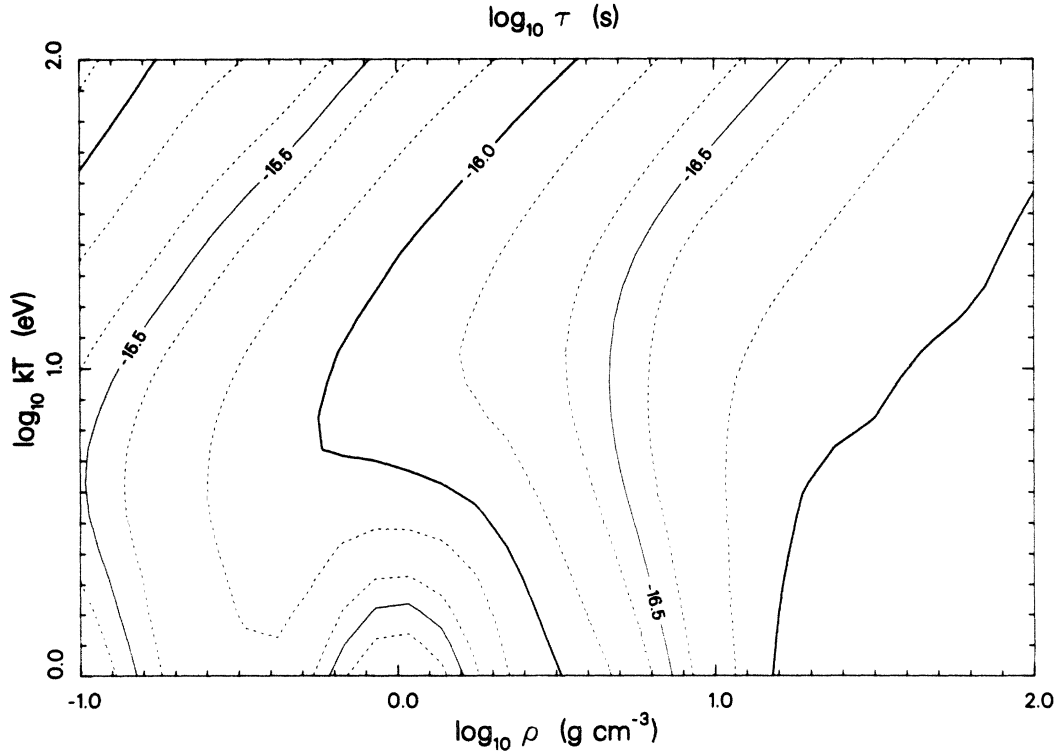

FIG. 12. Mean relaxation time τ of carbon near the conductor-insulator transitions, calculated with DFS potential configuration $1s^2 3d^3$.

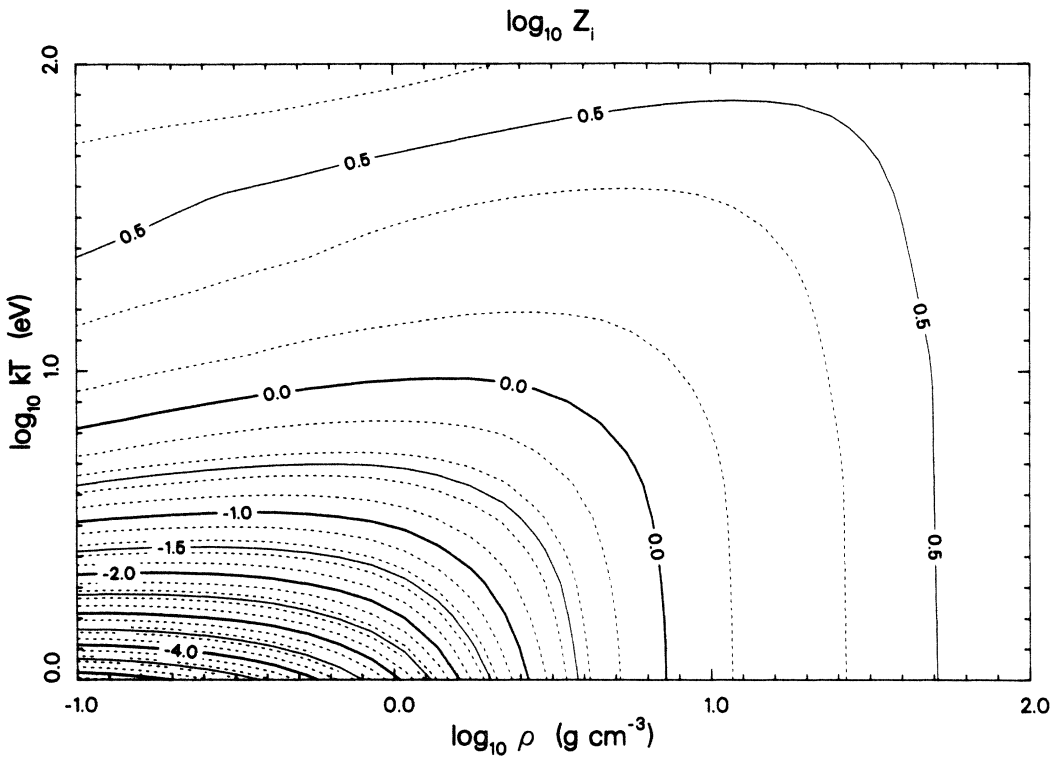

FIG. 13. Ionization state Z_i of carbon near the conductor-insulator transitions, calculated with DFS potential configuration $1s^2 2s^2 2p^1$.

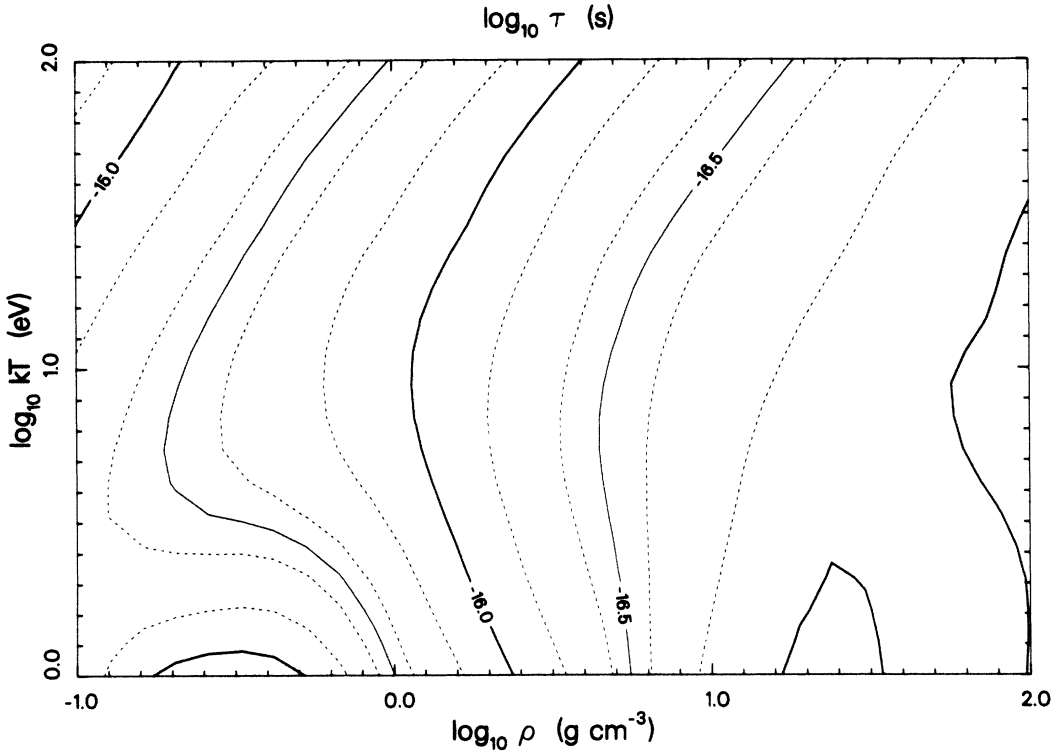

FIG. 14. Mean relaxation time τ of carbon near the conductor-insulator transitions, calculated with DFS potential configuration $1s^2 2s^2 2p^1$.

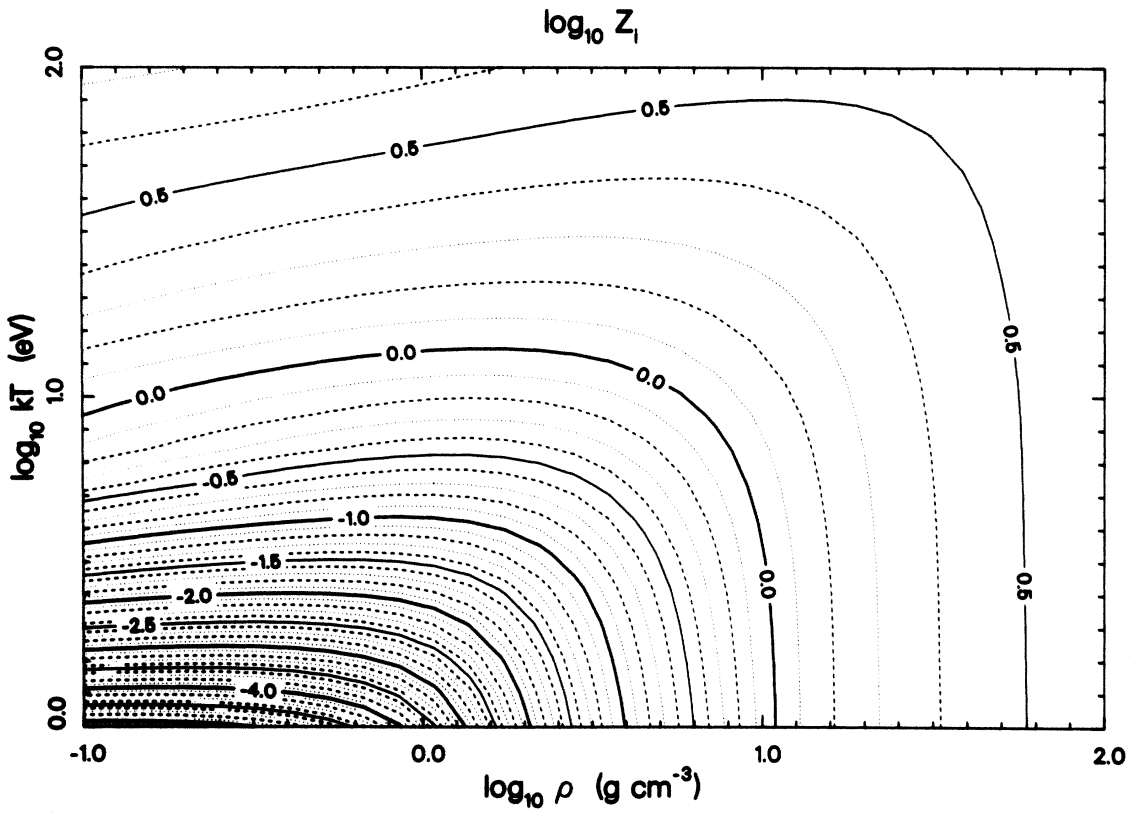

FIG. 15. Ionization state Z_i of carbon near the conductor-insulator transitions, calculated with DFS potential configuration $1s^2 3d^3$ and effects of linear fluctuations.

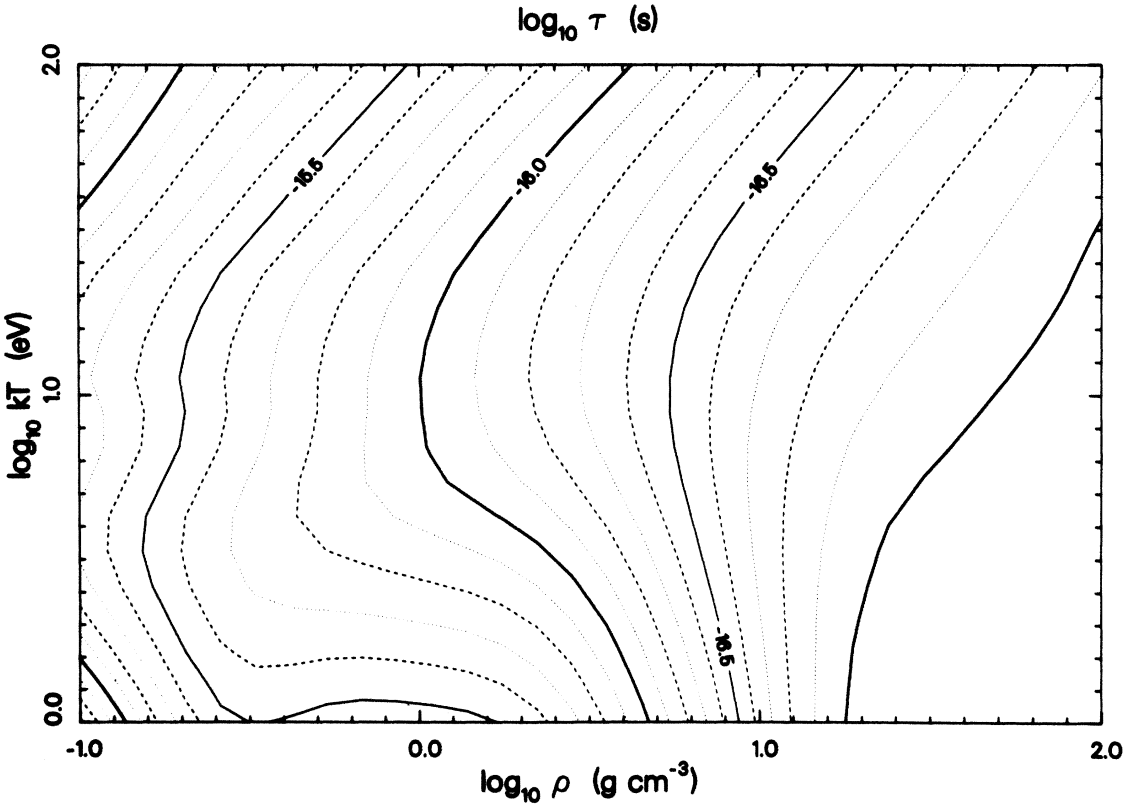

FIG. 16. Mean relaxation time τ of carbon near the conductor-insulator transitions, calculated with DFS potential configuration $1s^2 3d^3$ and effects of inverse fluctuations.

TABLE III. Ionization state $Z_i=Z_0$ and resistivity η ($\mu\Omega$ cm) for atomic numbers $Z=25-30$, at solid and liquid densities and temperatures as in Table I. Columns labeled "standard" are reference calculations from Table I. Columns labeled "convoluted" are modified with Eqs. (9) and (10), using the width $\gamma^{-1}=4r_t$ and the functions $g(p)=dN(\varepsilon)/d\varepsilon$ and $\Sigma(\varepsilon)$. Columns labeled "fluctuated" are modified with Eqs. (13)–(15).

	Solid						
	Expt.	Standard		Convoluted		Fluctuated	
$_ZX$	η	Z_i	η	Z_i	η	Z_i	η
$_{25}$Mn	185	0.71	240	0.86	184	0.73	139
$_{26}$Fe	10	0.53	81	0.72	88	0.58	146
$_{27}$Co	6	0.39	18	0.65	55	0.47	77
$_{28}$Ni	7	0.35	5	0.58	37	0.54	12
$_{29}$Cu	2	0.69	6	0.09	540	0.71	24
$_{30}$Zn	6	0.69	28	0.69	75	0.77	47
	Liquid (melting point)						
	Expt.	Standard		Convoluted		Fluctuated	
$_ZX$	η	Z_i	η	Z_i	η	Z_i	η
$_{25}$Mn	174	0.59	640	0.71	216	0.61	679
$_{26}$Fe	139	0.45	423	0.60	119	0.49	523
$_{27}$Co	102	0.29	281	0.48	78	0.36	506
$_{28}$Ni	85	0.20	440	0.79	83	0.32	214
$_{29}$Cu	21	0.57	45	0.51	86	0.54	98
$_{30}$Zn	37	0.60	90	0.60	171	0.69	177

standard results of Table I for $Z=25-30$ near normal conditions. In contrast to the situation at higher temperature, the effects are large and variable. At solid densities, no significant improvement is achieved by convolution except for manganese. Convolution produces remarkable improvement for the liquid transition metals but has the opposite effect for the liquid simple metals.

It is apparent that these adjustments have little effect in the regions of temperature-density space where we expect our theoretical model to be accurate in the first place. It is clear that they can improve agreement ir some cases near normal conditions, but that significant discrepancies remain. Effects of resonance broadening or fluctuations may account for some of the discrepancies in certain cases. However, the lack of systematic success shows that essential physical considerations are missing. We believe that a more careful treatment of geometrical and multiple-scattering effects is required in general in order to obtain quantitative results around normal conditions or near conductor-insulator transitions.

IV. TABLES OF TRANSPORT COEFFICIENTS

Numerical tables of ionization state Z_i, electrical conductivity σ (s^{-1}), thermal conductivity[5,10] κ ($cm^{-1}s^{-1}$), and thermoelectric coefficient[5,10] ξ ($cm^{-1}s^{-1}$) as functions of temperature kT (eV) and density ρ (g/cm^3) have been calculated for the entire Periodic Table by the theoretical methods described herein. The results are voluminous in general and may be obtained from the Los Alamos SESAME Library.[21] The coefficients are defined with respect to the transport equations

$$
\begin{aligned}
e\mathbf{J}&=\sigma\left[e\mathbf{E}+\frac{\Omega}{Z_i}\nabla P\right]+e^2\xi\frac{\nabla(kT)}{kT}\ ,\\
\mathbf{Q}&=-\xi\left[e\mathbf{E}+\frac{\Omega}{Z_i}\nabla P\right]-\kappa\nabla(kT)\\
&\quad-\frac{e^2\xi^2}{\sigma}\frac{\nabla(kT)}{kT}-\frac{5}{3}\frac{\langle\varepsilon\rangle}{e}\mathbf{J}\ ,
\end{aligned}
\tag{16}
$$

where $-e$ is the charge of the electron, and the other quantities are conventional. The thermoelectric coefficient ξ is related to the α coefficient of Spitzer and Härm[15] by $e\xi=\alpha T$. Further derivations, discussions of units, and sample tables have been published previously.[5–7,10] The tables are calculated on logarithmic grids in temperature-density space, with 20 temperature points from 10^{-2} to 10^4 eV, and 30 density points. These are then interpolated onto a finer mesh of 60 temperatures and 90 densities. For $Z\leq 3$, densities range from 10^{-4} to 10^5 g/cm^3; for $4\leq Z\leq 35$, from 10^{-3} to 10^6 g/cm^3; and for $36\leq Z$, from 10^{-2} to 10^7 g/cm^3. Tables are available both with and without the effects of fluctuations included. In some cases, additional tables have been constructed with empirical normalization to measurements in the vicinity of normal conditions. Normalization procedures include but are not limited to the semiempirical corrections discussed in Sec. III D. In general, we have adopted the ionization state convention $Z_i=Z_0$. However, other choices have been made and noted for empirically normalized tables. Redundant combinations of these parameters (conductive opacity, relaxation time, plasma frequency, etc.) are also available from the author in the same tabular form, as are some

related physical parameters (chemical potential, number of continuum electrons Z_c).

Within these ranges of temperature and density are substantial regions where the present physical model is invalid (see Fig. 3). Results have been retained in these regions for convenience of use. In the absence of experimental comparison, the accuracy of the tables may be monitored roughly by computing the ion-ion coupling constant $\Gamma = Z_i^2 \alpha \beta / r_t$ and the mean free path $\lambda = \tau p_F / m$. Where Γ is large ($\gtrsim 170$), the geometrical model is invalid and the transport coefficients should not be used, although the calculated ionization states may be reasonable. Where λ is of order r_t, the material is near the conductor-insulator transitions, and both the relaxation times and ionization states may be inaccurate. The only nontrivial parameter to be reconstructed here is the Fermi momentum p_F, which can be obtained through implicit solution of Eq. (3) for the chemical potential μ if the appropriate tables are not at hand.

The mean relaxation time τ may be reconstructed from Z_i and σ using Eq. (5) if conductivities corresponding to different values $Z_i \rightarrow Z_i'$ are desired. In effect, this renormalizes the electrical conductivity by a linear factor Z_i'/Z_i. In the Lorentz gas approximation, the thermal conductivity and thermoelectric coefficient are similarly renormalized. Here they are not strictly proportional to Z_i because the electron-electron interaction is included in the heat transport equations. In principle, the thermal transport coefficient should be reconstructed from the values of Z_i and σ actually adopted, but in practice, linear renormalization does not produce significant errors unless Z_i is changed radically.

ACKNOWLEDGMENTS

I would like to thank B. I. Bennett and J. E. Hammerberg for many hours of stimulating discussion throughout the course of this work, D. A. Liberman for generously contributing computer codes and ideas, G. Baym and J. D. Johnson for important additional insight, and R. L. Shepherd, L. A. Jones, I. R. Lindemuth, J. W. Shaner, and R. S. Hixson for making available their experimental results and analyses prior to publication.

[1] J. M. Ziman, *Principles of the Theory of Solids*, 2nd ed. (Cambridge University Press, Cambridge, 1972); J. M. Ziman, Philos. Mag. **6**, 1013 (1961).

[2] J. M. Ziman, *Electrons and Phonons* (Oxford University Press, Oxford, 1960).

[3] R. Evans, B. L. Gyorffy, N. Szabo, and J. M. Ziman, in *The Properties of Liquid Metals*, edited by S. Takeuchi (Wiley, New York, 1973).

[4] D. B. Boercker, F. J. Rogers, and H. E. DeWitt, Phys. Rev. A **25**, 1623 (1982).

[5] G. A. Rinker, Phys. Rev. B **31**, 4207 (1985); **31**, 4220 (1985); G. A. Rinker, Los Alamos National Laboratory Report No. LA-9872-MS, 1984 (unpublished); G. A. Rinker, Los Alamos National Laboratory Report No. LA-10202-MS, 1984 (unpublished).

[6] G. Rinker, Los Alamos National Laboratory Report No. LA-10608-MS, 1986 (unpublished).

[7] G. Rinker, Los Alamos National Laboratory Report No. LA-10404-MS 1985 (unpublished).

[8] L. E. Ballentine and J. E. Hammerberg, Can. J. Phys. **62**, 692 (1984).

[9] F. J. Rogers, D. A. Young, H. E. DeWitt, and M. Ross, Phys. Rev. A **28**, 2990 (1983).

[10] M. Lampe, Phys. Rev. **170**, 306 (1968); **174**, 276 (1968).

[11] D. A. Liberman, Phys. Rev. B **20**, 4981 (1979); J. Quant. Spectrosc. Radiat. Transfer **27**, 335 (1982).

[12] V. L. Moruzzi, J. F. Janak, and A. R. Williams, *Calculated Electronic Properties of Metals* (Pergamon, New York, 1978).

[13] G. Busch and H.-J. Güntherodt, in *Solid State Physics: Advances in Research and Applications*, edited by H. Ehrenreich, F. Seitz, and D. Turnbull (Academic, London, 1974), Vol. 29.

[14] R. L. Shepherd, Ph.D. thesis, University of Michigan, 1987 (unpublished); R. L. Shepherd, L. A. Jones, and D. R. Kania, Phys. Rev. Lett. (to be published).

[15] L. Spitzer, Jr., *Physics of Fully Ionized Gases* (Interscience, New York, 1962); L. Spitzer, Jr. and R. Härm, Phys. Rev. **89**, 977 (1953).

[16] S. Ichimaru, S. Mitake, S. Tanaka, and X.-Z. Yan, Phys. Rev. A **32**, 1768 (1985); S. Mitake, S. Tanaka, X.-Z. Yan, and S. Ichimaru, *ibid.* **32**, 1775 (1985); S. Tanaka, S. Mitake, X.-Z. Yan, and S. Ichimaru, *ibid.* **32**, 1779 (1985); X.-Z. Yan, S. Tanaka, S. Mitake, and S. Ichimaru, *ibid.* **32**, 1785 (1985); S. Ichimaru and S. Tanaka, *ibid.* **32**, 1790 (1985).

[17] Yu. V. Ivanov, V. B. Mintsev, V. E. Fortov, and A. N. Dremin, Zh. Eksp. Teor. Fiz. **71**, 216 (1971).

[18] V. K. Gryaznov, I. L. Iosilevskii, and V. E. Formov, Zh. Prikl. Mekh. Tekh. Fiz. **3**, 70 (1973); G. I. Kozlov and E. L. Stupitskii, *ibid.* **3**, 94 (1968); A. A. Likal'ter, Zh. Eksp. Teor. Fiz. **56**, 240 (1969).

[19] L. D. Landau and E. M. Lifshitz, *Statistical Physics*, 2nd ed. (Addison-Wesley, Reading, Mass., 1958).

[20] R. Landuaer, J. Appl. Phys. **23**, 779 (1952).

[21] SESAME Library, MS-B925, Los Alamos National Laboratory, Los Alamos, NM 87545.